Resting-state Brain Connectivity via Multivariate EMD in Mild Cognitive Impairment

Haifeng Wu, Lingxu Kong, Yu Zeng and Han Bao

Abstract: Mild cognitive impairment (MCI) is regarded as a brain disconnection syndrome. The functional connectivity from resting state functional magnetic resonance imaging (rs-fMRI) shows that the number and the strength of the connectivity in MCI will decrease. However, many studies have confirmed that, the decrease and increase in MCI actually coexist. This paper proposes a novel intrinsic-frequency connectivity to study the statistical significance between MCI and normal control (NC), especially stronger positive connectivity on an MCI group mean level. We use a multivariate empirical model decomposition to get intrinsic modal functions (IMFs) and calculate the correlations of the IMFs. In experiments, we use public data to test the proposed coefficient. When some dimension-reduction criteria are adopted, we can find some stronger intrinsic frequency correlation in MCI, which cannot be observed in traditional correlations. After further searched, the stronger connectivity is mainly distributed in the regions of MCI functional compensation and abnormal neuron recruitment hypothesis. From an intrinsic frequency spectrum, the reason for MCI's stronger positive intrinsic frequency correlation is that NC's correlation becomes smaller. One of explanations is that, the common respiration and cardiac noises in the intrinsic frequency correlation are removed, so that the positive correlation is weakened.

Keywords: rs-fMRI, functional connection, EMD, MCI

I. INTRODUCTION

Brain science shows that a brain performs conscious behaviors commonly in the cooperation of multiple brain regions, and functional connectivity (FC) can effectively express the cooperation relationship between the brain regions. At present, resting state functional magnetic resonance imaging (rs-fMR) is a popular method for the study of FC [1-4]. The imaging technology can measure the spontaneous activity of brain neurons without performing specific cognitive tasks, and thus study the default mode network (DMN) of a brain. FC plays an important role in the early detection and diagnosis of brain diseases. For example, as a common dementia, Alzheimer's disease (AD) manifests as mild cognitive impairment (MCI) in its early stages [5], and abnormalities can be detected from its DMN.

Pearson correlation method is a popular method to study FC [6-8], which extracts blood oxygen level dependent (BOLD) signals from several regions of interest (ROIs), and then calculates Pearson correlation coefficients between them to express the strength of connections and thus builds a connection network. This method is easy in calculation and operation, but if the BOLD signals exhibits non-stationarity, Pearson correlation is difficult to reflect the dynamic of the signals. For this reason, windowed Pearson coefficients can be calculated in several windows added to the BOLD signal [9]. However, the size of the windows will affect the coefficient performance of non-stationary signals [10]. Larger windows will produce lower temporal resolution. On the other hand, smaller window will also produce lower correlation coefficient resolution. More importantly, neither Pearson correlation nor windowed Pearson correlation focuses more on the connection strength at different frequencies. In fact, the firing rates of various brain neurons are different, and the frequency reflected from the BOLD signal is at a coarser scale than multi-electrode neuron recording [11]. The Pearson correlations above may not show FCs at different frequencies.

Wavelet methods can transform signals from a time domain to a time-scale domain and has been used in the FC study of rs-fMRI in recent years [11 12]. Since the wavelet methods can better perform time-frequency analysis of non-stationary signals, they can also show the time-frequency nature of a dynamic FC network. The methods are to perform wavelet transform on the BOLD signals of ROIs and then calculate the cross-power between them. However, the wavelet transform is much related to its mother function, and different mother functions will produce different results. Besides, there are numerous coefficients at different time and scale after wavelet transform. It is also a challenge to find features with statistical significance between experiment and control groups, from the numerous features. Reference [11] uses a maximum positive

This work was supported by the National Natural Science Foundation of China under Grant No. 61762093, the Key Application and Basic Research Fund of Yunnan Province under Grant 2018FA036, the Program for Innovative Research Team (in Science and Technology) in University of Yunnan Province, and the Science Research Fund Project of the Education Department of Yunnan Province under Grant 2020Y0238.

Haifeng Wu, LingXu Kong, Yu Zeng and Han Bao are with the School of Electrical and Information Engineering, Yunnan University for Nationalities, 650500 (email: whf5469@gmail.com, Kongloveslife@163.com, yv.zeng@gmail.com and 1298796915@qq.com)

coupling coefficient and a maximum phase difference criterion to find the FC features, but the number of obtained features is still large. In addition, the criterion cannot better reflect negative coupling coefficients. Existing study [12] has shown that the FC significance between groups is also in negative correlation.

MCI can be regarded as a kind of brain disconnection syndrome. Many studies [13, 14] have shown that the number and the strength of effective connections in MCI patients are lower than those of the NC group. However, there are also literatures [15, 16] that have confirmed that, as a pre-state of AD, the strengthening and weakening of functional connectivity actually coexist in MCI. Hypotheses such as functional compensation [15, 17] and abnormal neuron recruitment [18] are probable reasons for the increased connectivity between brain areas of MCI patients. In this paper, we will propose a novel FC coefficient, called intrinsic frequency correlation (IFC) for a statistical significance between a mild cognitive impairment (MCI) and a normal group with rs-fMRI, and especially focus on the connectivity where MCI group is stronger than NC. First, we extract BOLD series from ROIs and adopt a multivariate empirical model decomposition (MEMD) [19, 20] method to decompose these series into intrinsic model functions (IMFs) on layers. And then, we calculate the Pearson correlation matrices of the IMFs on the layers. Through the MEMD method, the BOLD series can be decomposed into IMFs with different frequencies, so that the correlation matrices from the IMFs can express the FC correlations at different frequencies. Furthermore, MEMD can make the decomposed IMFs from multiple channels match each other. Next, in order to find the significance between the two groups, we also use a minimum intra-class distance and a maximum inter-class distance criterion to reduce the dimensionality of IMF Pearson correlation.

In order to allow others to repeat our experiment , the data comes from the public rs-fMRI Alzheimer's Disease Neuroimaging Initiative (ADNI). Throughout the data, we give the experimental results of the intrinsic-frequency connectivity coefficient proposed in this paper. Adopting three dimension-reduction methods, some connectivity of MCI stronger than NC are observed in the proposed coefficient matrix, but these connections have not been observed in the traditional Pearson correlation and wavelet transform. To further find the distribution of the connectivity, we set up a search condition where MCI has a stronger positive correlation than NC. From the search results, the connectivity is mainly concentrated in the frontal, parietal, temporal and cerebellum. The first three are consistent with the region where MCI functional compensation [26-28] occurs, and the fourth region is consistent with the region of the MCI abnormal neuron recruitment hypothesis [18]. From the intrinsic-frequency spectrum, the intrinsic-frequency connectivity's difference between the MCI group and the NC group, is larger than the traditional Pearson correlation. The likely reason is that the intrinsic-frequencies correlation eliminates the common noise between ROIs caused by breathing and heartbeat [38-41], so that the positive correlation of NC is weakened and even becomes negative.

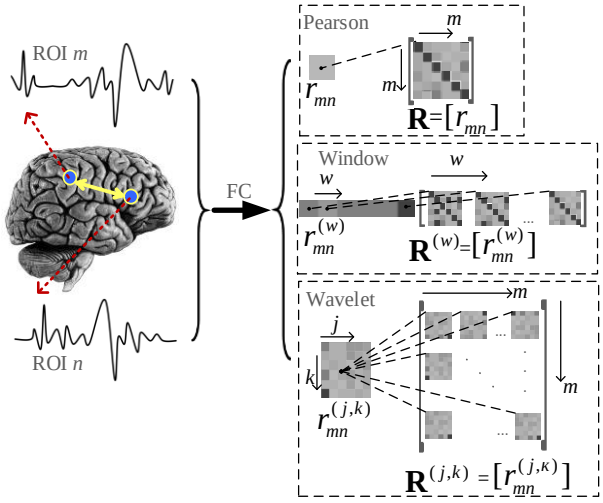

Fig. 1. Traditional FC correlation coefficients: Pearson correlation, windowed Pearson correlation and wavelet transform correlation

II. Related Work

In recent years, with the development of neuroimaging technology, non-invasive fMRI technology has been used more and more applied to brain science. In particular, rs-fMRI can show the DMN of a brain without completing any cognitive tasks. This can remove the impact of the tasks on the data, and thus is widely used in the study of FC. Pearson correlation coefficient [6-8] is earlier used to evaluate FC strength in a brain network. The coefficient calculates the correlation between the m-th ROI time series vector $\mathbf{X}_m=[x_{t,m}]\in\mathbb{R}^{T\times 1}$ and the n-th vector $\mathbf{X}_n=[x_{t,n}]\in\mathbb{R}^{T\times 1}$ and is shown as

$$r_{mn}=\frac{(\mathbf{X}_m-\mu_m)(\mathbf{X}_n-\mu_n)^{\mathrm{H}}}{\sqrt{(\mathbf{X}_m-\mu_m)(\mathbf{X}_m-\mu_m)^{\mathrm{H}}}\sqrt{(\mathbf{X}_n-\mu_n)(\mathbf{X}_n-\mu_n)^{\mathrm{H}}}} \tag{1}$$

where μ_m and μ_n represent the mean of series $\mathbf{X}_m$ and $\mathbf{X}_n$, respectively, $(\cdot)^{\mathrm{H}}$ enotes transpose. If the number of the extracted ROI series is M, the corresponding Pearson correlation matrix will be $\mathbf{R}=[r_{mn}]\in\mathbb{R}^{M\times M}$. A Comparison of the correlation matrix between an MCI group and an NC group, will find the difference in the connectivity between the two groups. At present, some deep learning algorithms, such as SAE [16] and CNN [21, 45 46], can extract the differences between the groups and use these differences to achieve good classification results.

Sometimes, the ROI time series shows non-stationarity. In this case, a time window can be added to calculate Pearson correlation for the dynamic of FC [17]. If $\mathbf{X}^{(w)}\in\mathbb{R}^{L\times 1}$ represents the series vector in the W-th window of the original vector $\mathbf{X}$, then the windowed Pearson correlation coefficient can be expressed as

$$r^{(w)}=\frac{(\mathbf{X}^{(w)}-\mu_x^{(w)})(\mathbf{Y}_t-\mu_y^{(w)})^{\mathrm{H}}}{\sqrt{(\mathbf{X}^{(w)}-\mu_x^{(w)})(\mathbf{X}^{(w)}-\mu_x^{(w)})^{\mathrm{H}}}\sqrt{(\mathbf{Y}^{(w)}-\mu_y^{(w)})(\mathbf{Y}^{(w)}-\mu_y^{(w)})^{\mathrm{H}}}} \tag{2}$$

where $\mu_x^{(w)}$ represents the mean of the series. Similar to the Pearson correlation matrix, W windowed Pearson

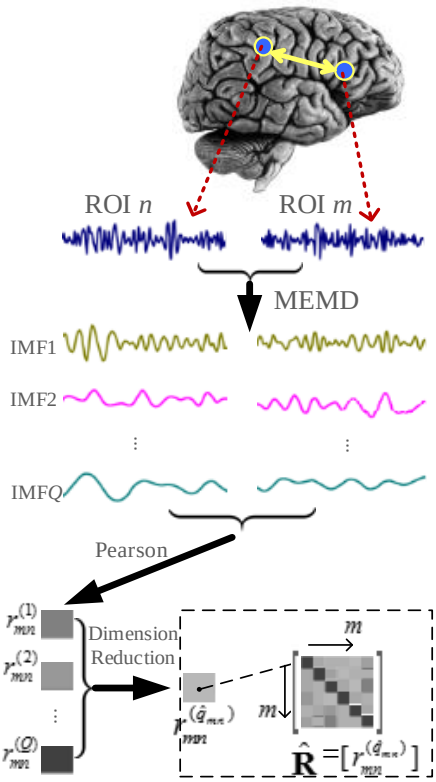

Fig. 2. The flowchart of IFC correlation coefficient

correlation matrices $\mathbf{R}^{(w)}=[r_{mn}^{(w)}] \in \mathbb{R}^{M\times M}$, w =1, 2, ... W can be produced. Compared with (1), the coefficient in (2) has a time variable, so it can express the change of the correlation with time.

Furthermore, in order to express the connection strength of FC at different frequencies, a wavelet transform method is also used in the study of FC. The general approach is to calculate a wavelet transform and then cross power of two ROI time series [11, 12, 22] to express the correlation between them, i.e.

$$r_{mn}^{(j,k)} = P_{xy}(WT_m^{(j,k)}, WT_n^{(j,k)}) \tag{3}$$

where

$P_{xy}(\cdot)$ is a cross power function,

$WT_m^{(j,k)} = \sum_t x_{t,m}\phi_{j,k}^*(t)$ is the signal after wavelet transform,

$\phi(t)$ is a wavelet mother function,

j and k are a scale and time factor, respectively,

$(\cdot)^*$ represents conjugate.

since the scale factor j make the wavelet function $\phi(t)$ lengthen or shorten, it can represent the frequency of a signal. Thus, the result in (3) on different j can express FC strength at different frequencies. Similar to the windowed Pearson, the correlation matrices on several scales and time factors would be $\mathbf{R}^{(j,k)}=[r_{mn}^{(j,k)}] \in \mathbb{R}^{M\times M}$, j=1, 2, ... J, k=1, 2, ... K。

III. Problem Description

Although Pearson correlation, windowed Pearson correlation and wavelet transform correlation coefficient can be expressed as the connection strength of FC, there are some problems when they are used to find a statistical significance between an MCI and NC group. Fig.1 illustrates the calculated FC strength between ROIs via the three methods above. Pearson correlation adopts all time points of two ROI series to calculate the coefficient r_{mn} as shown in (1), and produces a correlation matrix $\mathbf{R}$ when extending r_{mn} to multiple ROIs. However, the matrix does not contain any information about frequencies. For the windowed Pearson correlation $r_{mn}^{(w)}$ in (2) and its extended matrix $\mathbf{R}^{(w)}$, it has a time variable W, but still carry no information about frequencies. In fact, the Pearson correlation from the BOLD signal of ROI is within a frequency band. However, the value of the correlation at different frequencies may be different [11], and such Pearson correlation may conceal the statistical significance reflected at different frequencies.

In addition, the connection strength coefficient $r_{mn}^{(j,k)}$ via the wavelet transform does have time and frequency information. However, from (3), the final correlation will be a four-dimensional tensor $\mathbf{R}^{(j,k)}$, which has both a time variable k and a scale variable j. How to find features with statistical significance from the numerous coefficients is also a challenge. Reference [11] uses a maximum cross power spectrum and a maximum phase difference criterion to reduce the frequency dimension. Since there is no time dimension reduction, the number of coefficients is still large.

For the problem above, this paper proposes a novel correlation coefficient which can describe the FC connection strength at different frequencies. Besides, an intra-class and inter-class distance criterion is used to reduce the dimension of the coefficient. When using the dimension-reduction criteria, it can help us to find statistical significant between the MCI group and the NC at different intrinsic frequencies.

IV. IFC Correlation Coefficient

A. Overview of coefficient calculations

In this paper, we will use the proposed IFC coefficient to express the FC strength. The flow chart of the coefficient calculation is shown in Fig.2. First, extract the ROI time series from the rs-fMRI samples of subjects and let MEMD decompose each subject's ROI series into IMF components. Calculate each subject's Pearson correlation coefficient between each pair of ROIs on each layer of IMF. Finally, a dimension reduction criterion in training samples is used to decide which layer's IMF correlation should be selected for the final IFC coefficient. Next, we will give the details of the IFC calculation.

B. MEMD decomposition

For the IFC calculation, if EMD[47] decomposition is used

Table. 1.
Steps of calculating IFC correlation matrix

Input:
M ROI time series from a subject $\mathbf{X}_m = [x_{t,m}] \in \mathbb{R}^{T\times 1}$, $m = 1,2,..\ M$
Output:
IFC correlation coefficient matrix $\hat{\mathbf{R}} \in \mathbb{R}^{M\times M}$
Known:
There are N_I classes in a training set and each class contains N_J samples
Steps:
I MEMD
①Calculate the subject's Q IMF components $\mathbf{C}_m^{(q)} = [c_{t,m}^q] \in \mathbb{R}^{T\times 1}$, $m = 1,2,..\ M$, $q = 1,2,..\ Q$ from (4);
II IMF Correlation matrix
②Get the correlation matrix $\mathbf{R}^{(q)} = [r_{mn}^{(q)}] \in \mathbb{R}^{M\times M}$, $q = 1,2,..\ Q$ of each sample from equation (5-6);
III Dimensionality reduction
③Find the IMF component index $\hat{q}_{mn}$ in a training set by (9-13);
④Obtain the final correlation matrix $\hat{\mathbf{R}} = [\hat{r}_{mn}] \in \mathbb{R}^{M\times M}$ from (7-8).

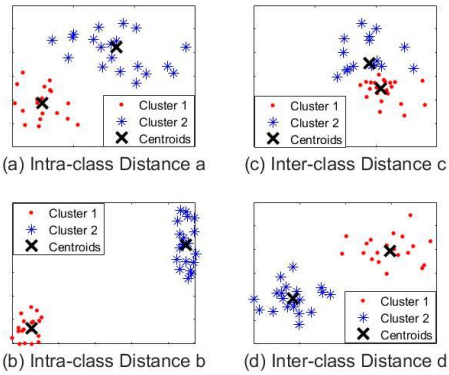

Fig. 3 Intra-class distance and inter-class distance in clustering, where intra-class distance in (a) > intra-class distance in (b) and inter-class distance in (c) < inter-class distance in (d)

independently for each ROI of each subject, it will cause the number of IMF components of each ROI to be different. It is difficult to calculate the correlation coefficient between each layer's IMFs because the IMFs on each layer probably do not match. MEMD [19, 20, 43, 44] is a multivariate (i.e. multi-channel) empirical mode decomposition, which can complete a joint decomposition of multiple ROI time series and make the IMF components of multiple ROI signals matched in time and layer. Therefore, this helps to calculate each layer's correlation. Let $\mathbf{X}_m = [x_{t,m}] \in \mathbb{R}^{T\times 1}$, $m = 1, 2, \ldots M$ be the time series of M ROIs extracted from a subject. After $\mathbf{X}_m$ is decomposed by MEMD, it can be expressed as

$$\mathbf{X}_m = \sum_{q=1}^{Q} \mathbf{C}_m^{(q)} + \mathbf{E}_m,\ m = 1, 2, \ldots M \tag{4}$$

where $\mathbf{C}_m^{(q)} = [c_{t,m}^q] \in \mathbb{R}^{T\times 1}$ is the q-th layer IMF vector and $\mathbf{E}_m$ is the residual. Through MEMD decomposition, it can be ensured that both $\mathbf{X}_m$ and $\mathbf{X}_n$ can be decomposed into Q IMF components, even if $m \neq n$.

C. IMF correlation coefficient matrix

After MEMD decomposition, the IMF components of multiple ROIs of each sample can be matched with each other, so the correlation coefficient matrix between these ROIs on each layer component can be calculated. The correlation coefficient between the m-th and the n-th ROI time series on the q-th layer IMF component can be expressed as

$$r_{mn}^{(q)} = \frac{(\mathbf{C}_m^{(q)} - \mu_m^{(q)})(\mathbf{C}_n^{(q)} - \mu_n^{(q)})^{\mathrm{H}}}{\sqrt{(\mathbf{C}_m^{(q)} - \mu_m^{(q)})(\mathbf{C}_m^{(q)} - \mu_m^{(q)})^{\mathrm{H}}}\sqrt{(\mathbf{C}_n^{(q)} - \mu_n^{(q)})(\mathbf{C}_n^{(q)} - \mu_n^{(q)})^{\mathrm{H}}}} \tag{5}$$

where $\mu_m^{(q)}$ represents the mean of the vector $\mathbf{C}_m^{(q)}$. If the number of ROIs is M, the correlation matrix on the q-th IMF component can be shown as

$$\mathbf{R}^{(q)} = [r_{mn}^{(q)}] \in \mathbb{R}^{M\times M},\ q = 1, 2, \ldots, Q \tag{6}$$

D. Dimensionality reduction

After MEMD and correlation calculation, there are Q correlation matrices for each subject. If these matrices are regarded as three-dimensional tensors, the dimension is $M \times M \times Q$. Here, we will use some criteria to reduce the third dimension Q. From $r_{mn}^{(q)}$, q =1, 2, … Q, select a correlation coefficient $r_{mn}^{(\hat{q}_{mn})}$ on the $\hat{q}_{mn}$-th layer component and let

$$\hat{r}_{mn} = r_{mn}^{(\hat{q}_{mn})} \tag{7}$$

Thus, we have the following correlation matrix after dimensionality reduction

$$\hat{\mathbf{R}} = [\hat{r}_{mn}] \in \mathbb{R}^{M\times M} \tag{8}$$

To find the component index $\hat{q}_{mn}$, we will use the following three criteria.

1) Minimum intra-class distance criterion

If there are N_I classes in a training set, the selection of $\hat{q}_{mn}$ in a minimum intra-class distance criterion will satisfy

$$\hat{q}_{mn} = \arg\min_{q\in\{1,2,..Q\}} \frac{1}{N_I}\sum_{i=1}^{N_I} \sigma_{mn}^{(q)}(i) \tag{9}$$

where $\sigma_{mn}^{(q)}(i)$ is defined as the intra-class distance of correlation coefficients in N_J training samples in the i-th class and the coefficients are for the q-th component correlation between the m-th and n-th ROIs, expressed as

$$\sigma_{mn}^{(q)}(i) = \frac{1}{N_J}\sum_{j=1}^{N_J} \sqrt{[r_{mn}^{(q)}(i,j) - \bar{r}_{mn}^{(q)}(i)]^2} \tag{10}$$

where $r_{mn}^{(q)}(i,j)$ represents the correlation coefficient of the j-th training sample in class i, and $\bar{r}_{mn}^{(q)}(i)$ corresponds to the mean of class i. The intra-class distance can represent the degree of aggregation of a class. Fig.3 (a) and (b) gives two kind of clustering results. From the figures, it can be seen that the intra-class distance of (b) is smaller than (a). Since the degree of aggregation in (b) is better, the classification in (b) is also easier.

2) Maximum inter-class distance criterion

If there are N_I classes in a training set, the selection of $\hat{q}_{mn}$ for a maximum inter-class distance criterion will satisfy

Table 2
Parameters in rs-fMRI data

Parameter	Philip
Equipment	
Field Strength	3.0 Tesla
Flip Angle	80 °
TR	3000ms
TE	30ms
Pixel Spacing	3.3mm ×3.3mm
Slices	48
Number of TR	140

$$\hat{q}_{mn} = \arg\max_{q\in\{1,2,..Q\}} \frac{1}{\binom{N_I}{2}} \sum_{i\neq j} \delta_{mn}^{(q)}(i,j) \tag{11}$$

where $\delta_{mn}^{(q)}(i,j)$ is defined as the inter-class distance of correlation coefficients between class i and j, and the coefficients are for the q-th component correlation between the m-th and n-th ROIs, expressed as

$$\delta_{mn}^{(q)}(i,j) = \sqrt{[\bar{r}_{mn}^{(q)}(i) - \bar{r}_{mn}^{(q)}(j)]^2} \tag{12}$$

The inter-class distance can represent the degree of difference between classes. Fig.3 (c) and (d) give two kind of clustering results. From the figures, it can be seen that the inter-class distance of (d) is greater than (c). Since the degree of difference in (d) is better, the classification in (d) is also easier.

3) Maximum intre-class minimum intra-class distance criterion

If there are N_I classes in a training set, the selection of $\hat{q}_{mn}$ in a maximum inter-class minimum intra-class distance criterion will satisfy

$$\hat{q}_{mn} = \arg\max_{q\in\{1,2,..Q\}} \frac{1}{\binom{N_I}{2}} \sum_{i\neq j} \delta_{mn}^{(q)}(i,j) \Big/ \frac{1}{N_I} \sum_{i=1}^{N_I} \sigma_{mn}^{(q)}(i) \tag{13}$$

Since (13) puts the inter-class distance on a numerator and the intra-class distance on a denominator, this criterion combines the two distance above.

The dimension of the correlation matrix $\hat{\mathbf{R}}$ obtained from (7-13) is $M \times M$. Compared with the windowed Pearson correlation and wavelet transform correlation matrix, the time dimension or frequency dimension will be reduced. In addition, the component index $\hat{q}_{mn}$ are usually different for different mn, i.e. $\hat{q}_{mn} \neq \hat{q}_{ij}$ when $mn \neq ij$. Since IMFs on different $\hat{q}_{mn}$ have different frequencies, $\mathbf{R}$ can reflect the connection strength between different pairs of ROIs at different frequencies. Moreover, the correlation coefficient $r_{mn}^{(\hat{q}_{mn})}$ selected by the above three criteria is not necessarily a positive coupling or negative coupling coefficient, but only represents correlation between a pair of ROIs at a frequency.

Finally, Table 1 shows the steps to calculate the IFC correlation matrix.

V. Experiment Setup

A. Data and preprocessing

In this experiment, we use MCI and NC rs-fMRI data collected by two different devices, Philip and Siemens. The data is from ADNI whose website is http://adni.loni. usc.edu/, and its parameter details are given in Table 2. Data preprocessing adopts Data Processing & Analysis of Brain Imaging (DPABI) toolbox [23]. The details are as follows.

- To ensure magnetization equilibrium, the first 10 rs-fMRI volumes are discarded for each subject collected by Philip, and 130 rs-fMRI volumes are retained; the first 17 rs-fMRI volumes are discarded for each subject collected by Siemens, and 180 rs-fMRI volumes are retained;
- In order to make the data on each slice correspond to the same time point, the slices are realigned with the 48th slice to minimize relative errors across each TR;
- Perform head motion correction and select the subjects with head motion less than 2.0 mm displacement in any directions or 2.0 of any angular motion throughout the resting-state scan ;

TABLE 3
PARAMETERS IN FC CORRELATION COEFFICIENTS

Parameters	**Description**
Pearson	
Correlation coefficient	Pearson correlation
Wavelet	
Wavelet generating function	Complex Morlet
Center frequency	1
bandwidth	1
Scale range	10-39
IFC[1]	
Dimension-reduction criterion	Minimum intra-class distance Maximum inter-class distance Min intra- and max inter-class distance

Note:
1. For IFC coefficient, the download address of MEMD code is https://github.com/mariogrune/MEMD-Python-

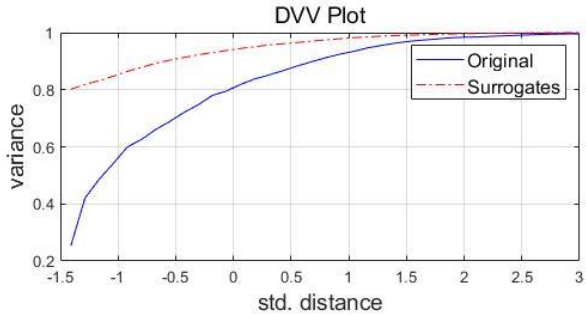

(a)

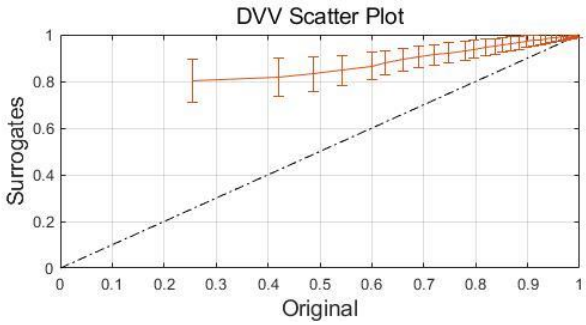

(b)

Fig. 4 (a) DVV plot and (b) DVV scatter plot by DVV toolbox [42], where 'original' denotes the ROI series and 'surrogate' denotes the surrogate signal through DVV toolbox.

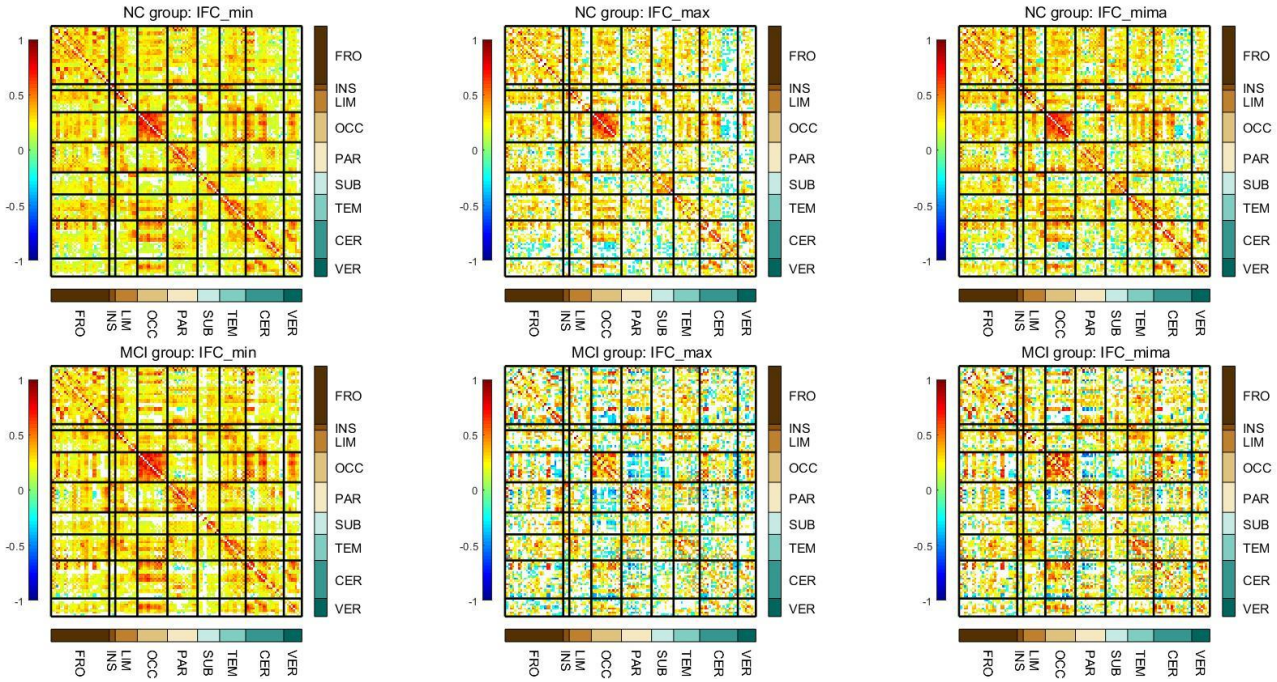

Fig. 5 Intrinsic-frequency connectivity: maximum inter-class distance (IFC_max, middle column), minimum intra-class distance (IFC_min, left column), and maximum inter-class & minimum intra-class distance (IFC_mima, right column); NC group means (top row), MCI group means (bottom row). Frontal = (1–16, 19–28, 69–70), insula = (29, 30); temporal = (79–90), parietal = (17–18, 57–68), occipital = (43–56), limbic = (31–40), subcortical = (41–42, 71–78), cerebellum = (91–108), vermis = (109–116), where No. of ROI is from AAL template, seen in Table A1 of Appendix. The white area is the points removed by FDR correction.

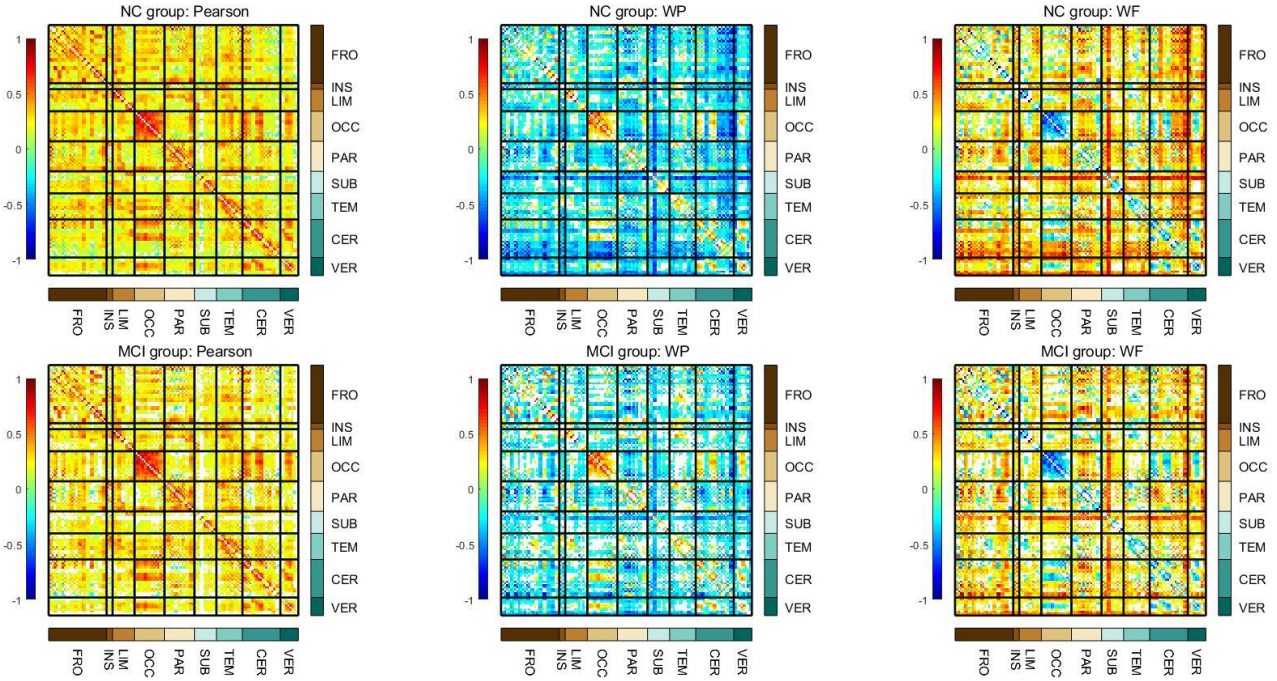

Fig. 6 Connectivity by Pearson correlation (right column) [16] and Wavelet method (middle column: WP, right column: WF) [11]: NC group means (top row) and MCI group means (bottom row). The ROIs are the same as Fig. 4 and the white area is the points removed by FDR correction.

- Perform reorientation on all subjects to prepare for the registration of rs-fMRI and MRI data ;
- The MRI data matching the rs-fMRI data performs skull stripping, and then registered with the rs-fMRI data so that the rs-fMRI data can be segmented into cerebrospinal fluid (CSF), gray matter and white matter (WM) signals ;
- Six motion parameters (i.e. three rotation parameters and three translation parameters), the CSF and WM signals are removed as nuisance variables to reduce the effects of head motion and non-neuronal BOLD fluctuations;

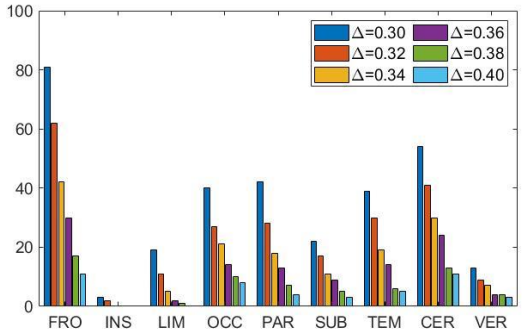

Fig. 7. Histograms of the number of the intrinsic frequency connectivity on group means: $MCI - NC > \Delta$ & $NC > 0$, where Δ =0.3-0.4.

- After normalization and smoothing, we fitter all data to a frequency range (0.01-0.08 Hz)
- Use Anatomical Automatic Labeling (AAL) [24] atlas to divide the brain into 116 ROIs and each hemisphere contains 58 regions; then, the Philip data matrix with 130×116 and the Siemens data matrix with 180×116 are obtained ;
- Select data from the image quality and registration quality of all subjects; finally, we obtain 32 MCI and 32 NC images scanned by Philip.

B. *Evaluated correlation coefficient*

This experiment compares the proposed IFC coefficient method with other conventional correlation coefficients, i.e. Pearson correlation coefficient (Pearson) [16], wavelet transform coupling coefficient [11]. The IFC coefficient method adopts three dimension reduction criteria, a minimum intra-class (IFC_min), a maximum inter-class (IFC_max) and a Minimum intra-class Maximum inter-class distance (IFC_mima) criterion to obtain three IFC coefficients. The details of the FC coefficients are as follows and their parameters are given in Table 3.

- Pearson：for ROI time series, calculate Pearson correlation coefficients in (1);
- Wavelet：after wavelet transforms of ROI time series, calculate the cross powers in (3) and perform dimension reduction through a maximum positive coupling value criterion in [11], get several wavelet coupling (WP) matrices / wavelet frequency (WF) disparity matrices on time points and then average them;
- IFC：steps are shown in Table 1 where IFC_min uses the minimum intra-class distance criterion, IFC_max uses the maximum inter-class distance criterion, and IFC_mima uses the maximum intre-class minimum intra-class distance criterion.

VI. RESULTS

A. *Correlation matrix: NC group and MCI group*

MEMD has its advantages in processing non-stationary and nonlinear signals, so it is necessary to determine whether the processed signal has nonlinearity. Here, we used the delay vector variance (DVV) toolbox [42] to test the time series extracted from the ROI. The test results are shown in Fig. 4.

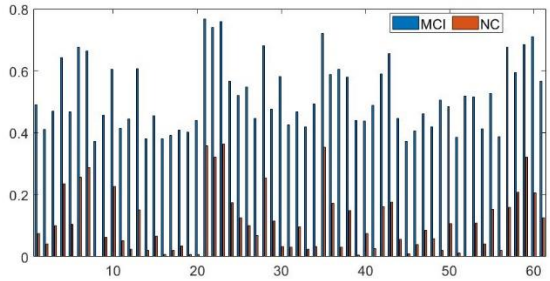

Fig. 8 Histograms of the intrinsic frequency connectivity between ROIs, for MCI (blue) and NC (red) group means: $MCI - NC > 0.36$ & $NC > 0$.

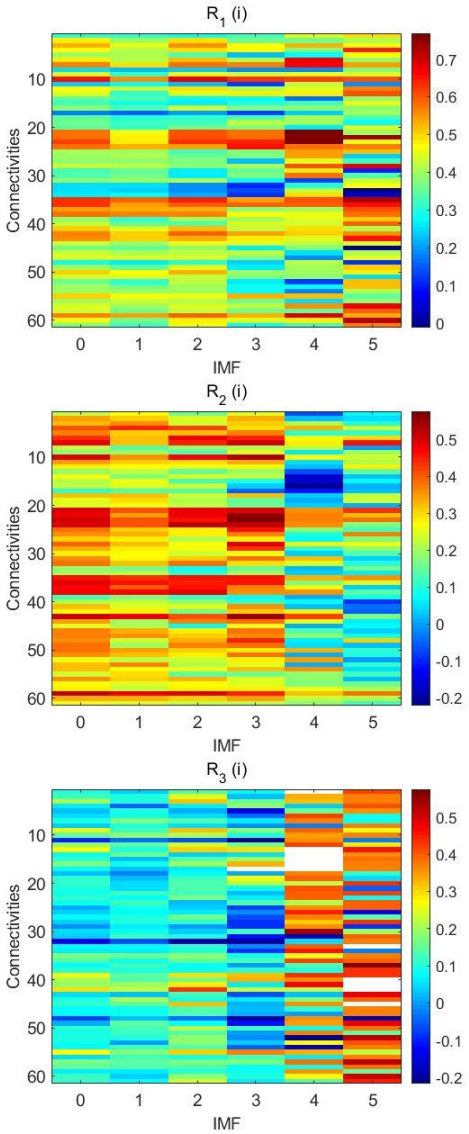

Fig. 9 Correlation coefficients for the connectivity in Fig. 7 on NC group means (middle) and MCI group means (top), and correlation difference ($\overline{MCI_i} - \overline{NC_i}$) on group means (bottom), where 0 on x-axis represents raw time series and 1-6 represent IMF 1-6, respectively.

Using the surrogate data methodology, the DVV plot in Fig. 4 (a) and the DVV scatter diagram in Fig. 4(b) can be generated using the DVV method. In DVV scatter diagram, the target variance values of the original signal are plotted against the averaged variance values, calculated over a number of

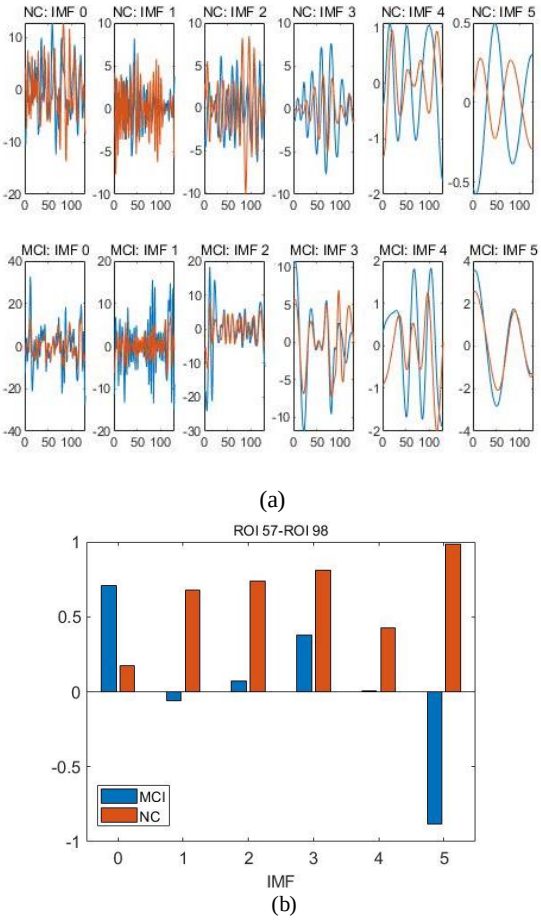

Fig. 10 An example of (a) raw time series and IMF 0-5 of ROI 57 (blue) and ROI 98(red) for an NC subject and an MCI subject, and (b) histograms of correlation coefficients of raw time series and IMF 0-5 for the NC subject (blue) and the MCI subject (red), where IMF 0 denotes the ROI raw time series.

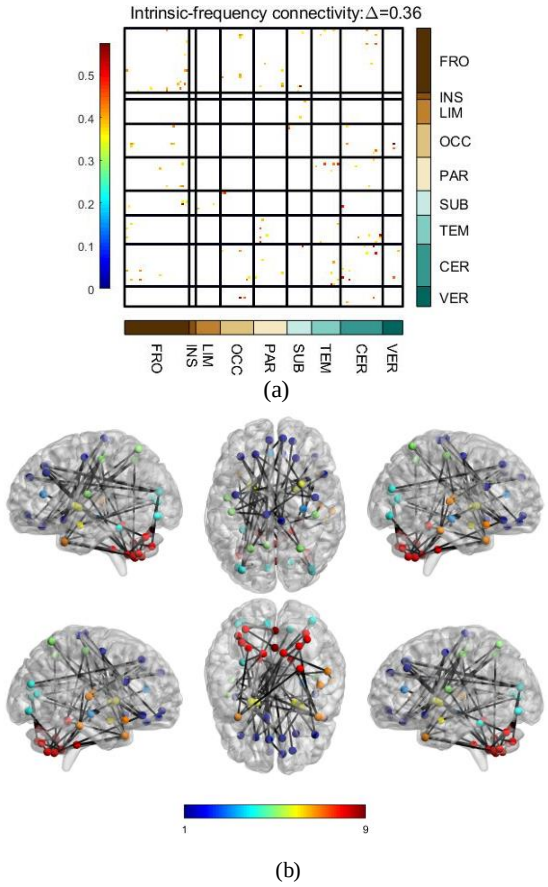

Fig. 11 (a) Intrinsic-frequency connectivity and (b) nodes and edges on group means: $\overline{MCI}$ - $\overline{NC}$ >0.36.& $\overline{MCI}$ >0 & $\overline{NC}$ >0.

surrogates. As a result, the scatter diagram deviates from bisector line. Thus, the tested data has the nonlinearity.

Fig. 5 shows the intrinsic-frequency correlation matrix from MEMD decomposition, on the NC and MCI group means. For comparison, Fig. 6 shows the correlation matrix of the Pearson and wavelet transform methods. For the Pearson correlation matrix, the frontal, occipital, and parietal regions have strong correlation. Since MCI is a brain disconnection syndrome, in general, the Pearson correlation of MCI is weaker than that of NC. For the WP correlation of the wavelet, the occipital region has stronger positive correlation, but other regions show more negative correlation patterns. In addition, the pattern of the WF correlation is opposite of WP. That is, the regions with a strong connectivity have a larger correlation value and a smaller frequency difference.

In Fig. 5, NC has stronger positive correlation than MCI in some regions, which is similar to the Pearson and wavelet in Fig. 6. However, in the regions connected with the frontal, temporal, parietal, and cerebellum, the MCI group has a stronger positive correlation than the NC group. The stronger positive correlations cannot be observed in the Pearson and wavelet. In the frontal connected with the occipital, for example, ROI 4 - 53 (SFGdor.R - IOG.L), ROI 23 -51 (SFGmed.L - MOG.L) and ROI 24 -54 (SFGmed.R - IOG.R), the MCI group is stronger than the NC group. These can be observed in all of the three criteria of MA, MI and MAMI.

B. Intrinsic frequency connectivity

To further analyze which regions in the MCI group have stronger intrinsic frequency correlation than the NC group, we set the following conditions

$$\overline{MCI} - \overline{NC} > \Delta \ \& \ \overline{NC} > 0 \tag{16}$$

where

$$\overline{MCI} - \overline{NC} = \max\{\overline{MCI}_i - \overline{NC}_i, i = 1, 2, \ldots\} \tag{17}$$

in which $\overline{MCI}_i$ and $\overline{NC}_i$ denote the i th IMF connectivity mean of the MCI and NC group, respectively and Δ is a threshold greater than 0. When Δ is 0.3-0.4, Fig. 7 shows the number of intrinsic frequency correlation coefficients that meet the condition (16) in the nine brain regions. No matter how Δ changes, the regions with more correlation coefficients meeting the condition are the frontal, occipital, parietal, temporal and cerebellum.

Next, we set the threshold in (16) to Δ = 0.36 to further analyze the intrinsic frequency correlations. It can be seen from Fig. 7 that if the threshold is too large, the number of intrinsic frequency correlation coefficients searched is too small, otherwise, it is too large, and 0.36 is a compromise. From the threshold, we find 61 intrinsic frequency correlations, and the mean values of their MCI and NC group are shown in Fig. 8.

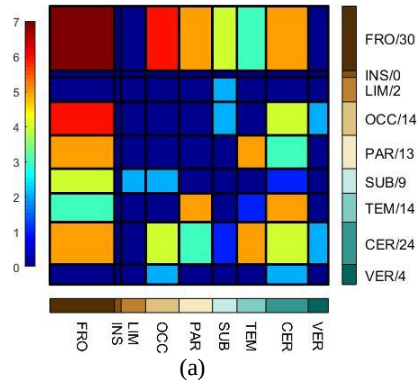

(a)

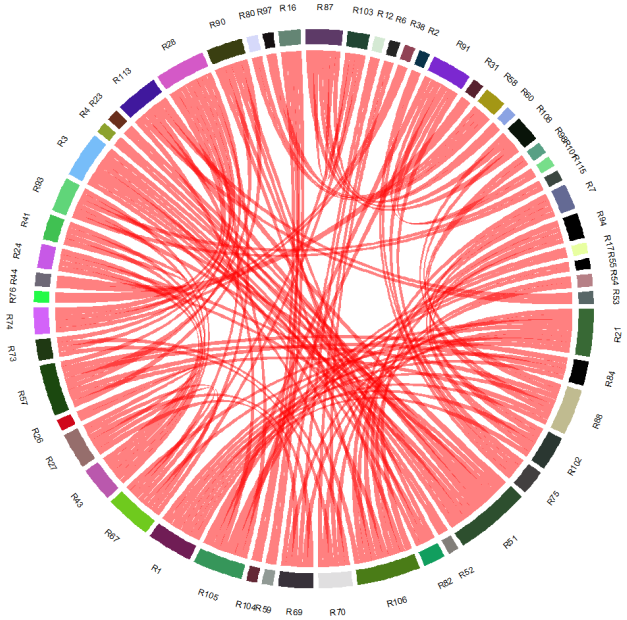

(b)

Fig. 12 (a) The numbers of Intrinsic-frequency correlations where the symbol'/' is followed by the number of correlations, and (b) topographical distribution of the 61 correlations in a circle plot, on group means: MCI - NC >0.36 & MCI >0 & NC >0.

Since the intrinsic frequency has different values on each IMF level, Fig. 9 gives their intrinsic-frequency spectrum, where we show each IMF's correlation coefficient $R_1(i)$, $R_2(i)$ on the MCI and NC group means of the above 61 correlations and the correlation coefficient difference $R_3(i)$ between the two groups. The relation is expressed as

$$R_1(i) = \overline{MCI}_i \tag{18}$$

$$R_2(i) = \overline{NC}_i \tag{19}$$

$$R_3(i) = \overline{MCI}_i - \overline{NC}_i \tag{20}$$

where i denotes the ith IMF component. If i is 0, it denotes the correlation of raw ROI time series, i.e. Pearson correlation. In the spectrum, most of the correlation coefficients and correlation coefficient differences increase with the value of i, that is, the correlation coefficient will have a larger value at a lower intrinsic frequency. In particular, the Pearson correlation calculated on the raw time series on the NC group is positive, while the correlation on some IMF components turns from positive to negative. Moreover, most of the correlation coefficient difference between groups does not reach the maximum value at i=0. This also means that the correlation coefficient on the IMF component may be larger than the Pearson correlation from the raw series.

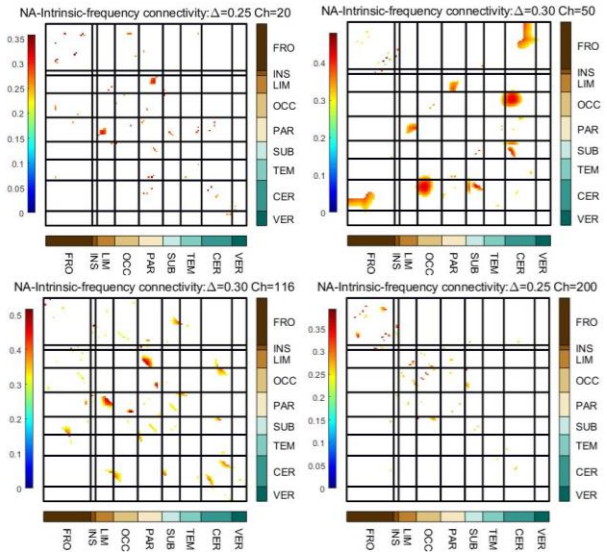

Fig. 13 Intrinsic-frequency connectivity by noise-assisted MEMD [44] : Δ =0.25 and ch =20 (top row and left column), Δ =0.30 and ch =50 (top row and right column), Δ =0.30 and ch =116 (bottom row and left column), Δ =0.25 and ch =200 (bottom row and right column), where ch denotes the number of noise channels, the noise is selected as Gaussian white noise and the signal to noise ratio is 0dB.

Fig. 10 shows an example for calculating the intrinsic frequency correlation spectrum. In the example, the time series of ROI 57 and 58 of an MCI subject and an NC subject are extracted respectively, and the series are decomposed by MEMD to get IMF 0-5. Then, the correlation coefficients on the raw time series and each IMF component is calculated. In the figure, the correlation of the raw time series on the NC subject is weaker than that of the MCI subject, and the difference between the two is about 0.5. On the other hand, the difference of the correlation coefficients between the NC and MCI subjects on each IMF component shows diversity. Similar to the correlation coefficient of the raw sequence, the correlation value of IMF2, 3 and 4 in the NC subject is positive, and the correlation value of MCI is also positive. However, the difference between the correlation values of NC and MCI subjects on each IMF is not the same. The difference on IMF2 is the largest, reaching about 0.7, larger than the correlation of the raw time series. Besides, note that for IMF1 and IMF5, the NC subject has a negative correlation, while its raw time series has a positive correlation. That is, raw Pearson correlation may change from positive to negative after EMD decomposition.

To facilitate visualization, the distribution of the 61 correlations on a correlation matrix is shown in Fig. 11(a), and the edges of these correlation are displayed in BrainNet Viewer [25] in Fig. 11(b). Consistent with the results in Fig. 7, except the regions correlated to the limbic, subcortical and vermis,

where the number of the correlation coefficients satisfying (11) is less, the other regions are more.

In order to count the number of correlation coefficients in each region, we give Fig. 12(a). In the figure, the regions correlated to the frontal, occipital, parietal, temporal, and cerebellum have more correlations, 30, 14, 13, 14 and 24, respectively. Fig. 12(b) uses a circle plot to show the 61 connections, where the arc with larger length has more connections. In the figure, R51 (left middle occipital gyrus, MOG) has the largest arc lengths. The connections are mainly distributed with R3 (left/right superior frontal gyrus dorsal, SFGdor), and 23 (left superior frontal gyrus middle, SFGmid).

From literatures [19, 20, 43, 44], a noise-assisted MEMD can reduce the mode mixing. Here, we recalculated the correlation using the noise-assisted method in [44]. First, use the noise-assisted MEMD to decompose the ROI signals, and then compute the intrinsic frequency correlations on IMFs. We give the comparison results from the method. For the noise-assisted method, the noise is selected as Gaussian and the signal-to-noise ratio is 0dB. According to the literatures [19, 43], the number of channels of noise should be a compromise value. Too large can reduce mode mixing, but it will also cause leakage. Here, we choose four channel numbers, 20, 50, 116 and 200, respectively. From Fig. 13, after the noise-assisted method used, the searched points are more concentrated, not as scattered as the points in the noiseless-assisted method, and the distribution of these points looks like some clusters. Although the results are different from the noiseless-assisted results, the distribution area is still concentrated in the cerebellum, the frontal and the occipital.

VII. Conclusion and Discussion

This paper proposes a method of intrinsic-frequency connection to study the functional connectivity of rs-fMRI. This method first extracts the ROI time series from each subject using the AAL template, and then simultaneously performs multi-channel empirical mode decomposition on the ROI time series to get IMF components. Finally, it calculates the correlation coefficient on each IMF. Through the data from ADNI, we used this method to calculate the intrinsic frequency connection of the MCI and NC group, focusing on the differences between the two groups. And the differences are difficult to be observed in the traditional methods like the Pearson correlation or the wavelet.

In the proposed method, we use three criteria, maximum inter-class distance, minimum intra-class distance and maximum intra-class maximum inter-class distance to reduce the dimension of the intrinsic-frequency correlation matrix, respectively and get the correlation matrices on the MCI and NC group mean level. The three matrices all show that some MCI connections have stronger positive correlation than NC, for example, the correlations between ROI 4 - 53 (SFGdor.R - IOG.L), ROI 23 -51 (SFGmed.L - MOG.L) and ROI 24 -54 (SFGmed.R - IOG.R), which are not observed in the traditional Pearson and wavelet correlation matrix.

We analyzed the spectra for the intrinsic frequency correlation on MCI and the NC group mean, and the spectra for the difference between the two groups. Compared with the Pearson correlation from raw series, the MCI group's intrinsic-frequency correlations are indeed stronger on some IMF layers, while the NC group's connection is weaker. Thus, the difference between the two groups is larger than the Pearson correlation. And, the correlations with larger differences mostly occur at lower intrinsic frequencies (higher IMF layers). Some intrinsic frequency correlations of the NC group have weaker positive correlations than the Pearson correlations of the raw series. One of likely explanations is that the raw series have the common noise, from respiration and cardiac processes [38-41], which make the correlation between regions tends to be positive. However, the series decomposed by MEMD are at different intrinsic frequencies. When there is no common noise at the intrinsic frequency of some IMFs, the positive correlation will be weakened, and even will appear negative. The factors will make it easier to find stronger connections of the MCI group than those of the NC through the intrinsic frequency connection, instead of the Pearson correlation.

To find where the correlation coefficients with stronger positive correlation are, we set the search condition, where the mean intrinsic frequency correlations of the MCI and NC group are positive and the differences between the two groups are greater than a threshold. We set the threshold between 0.3-0.4. No matter how the threshold changes, the searched correlations are mostly distributed in the regions correlated to the frontal, cerebellum, temporal, occipital, and parietal.

Moreover, to further analyze the correlations, we set the threshold to 0.36, because a larger threshold will result in fewer search results, and vice versa. From the threshold, 61 correlations coefficients with stronger positive correlation are found. For the coefficients, we still find that the correlation coefficients are distributed in the frontal, cerebellum, temporal, occipital, and parietal, from the highest to the lowest. The number of coefficients is 30, 24, 14, 14 and 13, respectively. The frontal, temporal and parietal are consistent with the regions [29-32] where the cognitive function loss compensation hypothesis [26-28] occurs in MCI, and the number and the value of the correlation coefficients both are enhanced. For the occipital, the positive correlation coefficients appear in the correlated frontal, about 6 out of the 14, and the frontal is also the region with the cognitive function loss compensation. Besides, it is interesting that the cerebellum has many strong positive correlation coefficients. The region is one of the common areas of the resting state network (RSN). There are many evidences that it is also involved in various cognitive impairment including MCI and AD [28, 30, 33-35]. Although the cerebellum usually does not have amyloid plaques [36, 37], MCI can cause changes in the primary cerebral cortex. This will result in abnormal recruitment of neurons and affects the change of RSN and the increase of the connectivity in the cerebellum, which is confirmed in literature [18].

In addition, the noise-assisted results are similar to the noiseless-assisted ones, and the searched regions are still concentrated in the cerebellum, the frontal and the occipital. The likely explanation for the similar results obtained by noise-assisted MEMD algorithm is that the ROI series themselves are noisy. Therefore, direct MEMD decomposition for the ROI is

equivalent to adding noise to a pure signal and then performing MEMD decomposition. This algorithm is actually similar to MEMD decomposition with several noise channels. Both of them are to prevent mode splitting.

In the method of the empirical mode method, one of problems is how to match on IMF layers. When MEMD decomposes multiple ROI series of a subject simultaneously, the number of IMF layers decomposed is the same. Since each subject uses MEMD to decompose its ROI independently, however, the number of IMF decomposed between subjects will be different. In this case, it is difficult to ensure that one IMF correlation of one subject matches that of another subject. One solution is to use MEMD for all ROIs of all subjects simultaneously, instead of all ROIs of each subject independently. However, this will cause the number of MEMD's channels to increase significantly. When the channels increases, the higher-layer IMF components tend to be the same due to the Hamersley sequence [19] by MEMD. In this case, the correlation coefficient on higher layers will be closer to 1, and it will be more difficult to find the statistical significance. To ensure that the number of IMF layers of all subjects is the same in the experiment, the final number of layers selects the minimum of the number of IMF layers of all subjects. Then, the group mean of each layer is the mean of the correlation coefficients calculated on the same layer. Although they may not match strictly, unlike Fourier transform and wavelet transform, the frequency of the IMF component by EMD is the intrinsic frequency of a signal, which is usually a frequency range rather than a point. Therefore, the correlation coefficient calculated in this way does not represent a frequency value, but a frequency band. Matching in a frequency range is much looser than that at a frequency point.

Furthermore, to find the differences unobserved in the traditional methods, the focus of this paper is that MCI has stronger correlation than NC. In fact, we can also study some other differences, e.g. the connectivity of NC with negative correlation. As mentioned above, the negative correlation of NC is easily ignored, due to the common respiration and cardiac noise in raw series. In the future, we can use the EMD method to find intrinsic frequency connectivity with stronger negative correlation between the MCI and the NC group.

The algorithm code and processed data in this paper have been uploaded to GitHub, and its download address is https://github.com/monk5469/MEMD_MCI_fMRI.

APPENDIX

This appendix gives the indices and names of the ROIs in the AAL template, seen in Table A1.

REFERENCES

[1] Phinyomark, A., Ibanez-Marcelo, E., & Petri, G., "Resting-State fMRI Functional Connectivity: Big Data Preprocessing Pipelines and Topological Data Analysis," IEEE Transactions on Big Data, vol. 3, no. 4, pp. 415–428, Dec. 2017.

[2] Cai, B., Zhang, G., Zhang, A., Stephen, J. M., Wilson, T. W., Calhoun, V. D., & Wang, Y., "Capturing Dynamic Connectivity from Resting State fMRI using Time-Varying Graphical Lasso," IEEE Transactions on Biomedical Engineering, vol. 66, no. 7, pp. 1852–1862, Jul. 2019.

[3] Rahim, M., Thirion, B., Comtat, C., & Varoquaux, G., "Transmodal Learning of Functional Networks for Alzheimer's Disease Prediction," IEEE Journal of Selected Topics in Signal Processing, vol. 10, no.7, pp. 1204–1213, Oct. 2016.

[4] Wang, M., Jie, B., Bian, W., Ding, X., Zhou, W., Wang, Z., & Liu, M., "Graph-Kernel Based Structured Feature Selection for Brain Disease Classification Using Functional Connectivity Networks," IEEE Access, vol. 7, pp. 35001–35011, Mar. 2019.

Table A1
The indices and names of the ROIs in the AAL template. The odd and even indices refer, respectively, to the left- and right-hemispheric regions.

Index	ROI label	Index	ROI label
1,2	PReCentral cyrus (PReCG)	3,4	Superior frontal gyrus (dorsal) (SFGdor)
5,6	ORBitofrontal cortex (superior) (ORBsupb)	7,8	Middle frontal gyrus (MFG)
9,10	ORBitofrontal cortext (middle) (ORBmid)	11,12	Inferior frontal gyrus (opercular) (IFGoperc)
13,14	Inferior frontal gyrus (triangular) (IFGtrang)	15,16	ORBitofrontal cortex (inferior) (ORBinf)
17,18	ROLandic operculum (ROL)	19,20	Supplementary motor area (SMA)
21,22	OLFactory (OLF)	23,24	Superior frontal gyrus (middle) (SFGmed)
25,26	ORBitofrontal cortex (medial) (ORBmed)	27,28	RECtus gyrus (REC)
29,30	INSula (INS)	31,32	Anterior cingulate gyrus (ACG)
33,34	Middel cingulate gyrus (MCG)	35,36	Posterior cingulate gyrus (PCG)
37,38	Hippocampus (HIP)	39,40	Parahippocampal gyrus (PHG)
41,42	AMYGdala (AMYG)	43,44	CALcarine cortex (CAL)
45,46	CUNeus (CUN)	47,48	LINGual gyrus (LING)
49,50	Superior occipital gyrus (SOG)	51,52	Middle occipital gyrus (MOG)
53,54	Inferior occipital gyrus (IOG)	55,56	FusiForm gyrus (FFG)
57,58	PostCentral gyrus (PoCG)	59,60	Superior parietal gyrus (SPG)
61,62	Inferior parietal lobule (IPL)	63,64	SupraMarginal gyrus (SMG)
65,66	ANGular gyrus (ANG)	67,68	PreCUNeus (PCUN)
69,70	ParaCentral lobule (PCL)	71,72	CAUdate (CAU)
73,74	PUTamen (PUT)	75,76	PALlidum (PAL)
77,78	THAlamus (THA)	79,80	HESh1 gyrus (HES)
81,82	Superior temporal gyrus (STG)	83,84	Temporal POle (superior) (TPOsup)
85,86	Middel temporal gyrus (MTG)	87,88	Temporal POle (middle) (TPOmid)
89,90	Inferior temporal gyrus (ITG)	91–94	Crus I-II of cerebellar hemisphere (Crus)
95–108	Lobule III-X of cerebellar hemisphere (Lobule)	109–116	Lobule I-X of vermis (vermis)

Frontal = (1–16, 19–28, 69–70); insula = (29:30); temporal = (79–90); parietal = (17–18, 57–68); occipital = (43–56); limbic = (31–40); subcortical = (41–42, 71–78); cerebellum = (91–108); vermis = (109–116)

[5] Binnewijzend, M. A. A., Schoonheim, M. M., Sanz-Arigita, E., Wink, A. M., van der Flier, W. M., Tolboom, N., … Barkhof, F., "Resting-state fMRI changes in Alzheimer's disease and mild cognitive impairment," Neurobiology of Aging, vol. 33, no. 9, pp. 2018–2028, Sept. 2012.

[6] Pannunzi, M., Hindriks, R., Bettinardi, R. G., Wenger, E., Lisofsky, N., Martensson, J., … Deco, G., "Resting-state fMRI correlations: From link-wise unreliability to whole brain stability," NeuroImage, vol. 157,pp. 250–262, Aug. 2017.

[7] Wang, S., Zhan, Y., Zhang, Y., Lyu, L., Lyu, H., Wang, G., … Guo, W., "Abnormal long- and short-range functional connectivity in adolescent-onset schizophrenia patients: A resting-state fMRI study," Progress in Neuro-Psychopharmacology and Biological Psychiatry, vol. 81, pp. 445–451, Feb. 2018

[8] Zhang, W., Liu, X., Zhang, Y., Song, L., Hou, J., Chen, B., … Lii, H., "Disrupted functional connectivity of the hippocampus in patients with hyperthyroidism: Evidence from resting-state fMRI," European Journal of Radiology, vol. 83, no. 10, pp. 1907–1913, Oct. 2014.

[9] Damaraju, E., Allen, E. A., Belger, A., Ford, J. M., McEwen, S., Mathalon, D. H., … Calhoun, V. D., "Dynamic functional connectivity analysis reveals transient states of dysconnectivity in schizophrenia," NeuroImage: Clinical, vol. 5, pp. 298–308, Jul. 2014.

[10] Canal, M. R., "Comparison of Wavelet and Short Time Fourier Transform Methods in the Analysis of EMG Signals," Journal of Medical Systems, vol. 34, no. 1, pp. 91–94, Oct. 2008.

[11] Miller, R. L., Yaesoubi, M., & Calhoun, V. D., "Cross-Frequency rs-fMRI Network Connectivity Patterns Manifest Differently for Schizophrenia Patients and Healthy Controls," IEEE Signal Processing Letters, vol. 23, no. 8, pp. 1076–1080, Aug. 2016.

[12] Chang, C., & Glover, G. H., "Time–frequency dynamics of resting-state brain connectivity measured with fMRI," NeuroImage, vol. 50, no. 1, pp. 81–98, Mar. 2010.

[13] Xiaowei Zhang, Bin Hu, Xu Ma, Linxin Xu, "Resting-State Whole-Brain Functional Connectivity Networks for MCI Classification Using L2-Regularized Logistic Regression," IEEE Transactions on NanoBioscience, Vol. 14, No. 2, pp. 237–247, 2015

[14] Laia F., Joan G., Maribel P., "Mild cognitive impairment and fMRI studies of brain functional connectivity: the state of the art," Frontiers in Psychology, Vol. 6, pp. 1095, 2015

[15] Liang P. , Wang Z., Yang Y., Jia X., Li K., "Functional Disconnection and Compensation in Mild Cognitive Impairment: Evidence from DLPFC Connectivity Using Resting-State fMRI," PLoS ONE, Vol. 6, No. 7, pp. e22153, 2011

[16] R. Ju, C. Hu, p. zhou and Q. Li, "Early Diagnosis of Alzheimer's Disease Based on Resting-State Brain Networks and Deep Learning," IEEE/ACM Transactions on Computational Biology and Bioinformatics, vol. 16, no. 1, pp. 244-257, 1 Jan.-Feb. 2019.

[17] Suk, H.-I., Wee, C.-Y., Lee, S.-W., & Shen, D., "State-space model with deep learning for functional dynamics estimation in resting-state fMRI," NeuroImage, vol. 129, pp. 292–307, Apr. 2016.

[18] Gloria Castellazzi, et al., "A comprehensive assessment of resting state networks: bidirectional modification of functional integrity in cerebro-cerebellar networks in dementia," Frontiers in Neuroscience, Vol. 8, pp. 23, 2014

[19] Ur Rehman, N., & Mandic, D. P., "Filter Bank Property of Multivariate Empirical Mode Decomposition," IEEE Transactions on Signal Processing, vol. 59, no. 5, pp. 2421–2426, May. 2011.

[20] S. Farahmand, T. Sobayo and D. J. Mogul, "Noise-Assisted Multivariate EMD-Based Mean-Phase Coherence Analysis to Evaluate Phase-Synchrony Dynamics in Epilepsy Patients," IEEE Transactions on Neural Systems and Rehabilitation Engineering, vol. 26, no. 12, pp. 2270-2279, Dec. 2018.

[21] T. Kam, H. Zhang, Z. Jiao and D. Shen, "Deep Learning of Static and Dynamic Brain Functional Networks for Early MCI Detection," IEEE Transactions on Medical Imaging, vol. 39, no. 2, pp. 478-487, Feb. 2020.

[22] Yaesoubi, M., Allen, E. A., Miller, R. L., & Calhoun, V. D., "Dynamic coherence analysis of resting fMRI data to jointly capture state-based phase, frequency, and time-domain information," NeuroImage, vol. 120, pp. 133–142, Oct. 2015.

[23] Y. Chao-Gan, Z. Yu-Feng, "DPARSF: a MATLAB toolbox for pipeline data analysis of resting-state fMRI," Frontiers in systems neuroscience, vol. 4, 2010.

[24] Tzourio-Mazoyer, Nathalie, et al., "Automated Anatomical Labeling of Activations in SPM Using a Macroscopic Anatomical Parcellation of the MNI MRI Single-Subject Brain," NeuroImage, vol. 15, no. 1, pp. 273–289, 2002.

[25] M. Xia, J. Wang and Y. He, "BrainNet Viewer: a network visualization tool for human brain connectomics," PloS one, vol. 8, no. 7, 2013.

[26] Grady, C.L., McIntosh, A.R., Beig, S., Keightley, M.L., Burian, H., Black, S.E., "Evidence from functional neuroimaging of a compensatory prefrontal network in Alzheimer's disease," J. Neurosci, Vol. 23, No. 3, pp. 986–993, Feb, 2003.

[27] Celone, K.A., Calhoun, V.D., Dickerson, B.C., Atri, A., Chua, E.F., Miller, S.L., DePeau, K., Rentz, D.M., Selkoe, D.J., Blacker, D., Albert, M.S., Sperling, R.A., "Alterations in memory networks in mild cognitive impairment and Alzheimer's disease: an independent component analysis," J. Neurosci., Vol. 26, No. 40, pp. 10222–10231, Oct, 2006.

[28] Bai, F., Watson, D.R., Yu, H., Shi, Y., Yuan, Y., Zhang, Z., "Abnormal resting-state functional connectivity of posterior cingulate cortex in amnestic type mild cognitive impairment," Brain Res, Vol. 1302, pp. 167–174, Dec, 2009.

[29] Das, S.R., Pluta, J., Mancuso, L., Kliot, D., Orozco, S., Dickerson, B.C., Yushkevich, P.A., Wolk, D.A., "Increased functional connectivity within medial temporal lobe in mild cognitive impairment," Hippocampus Vol. 23, No. 1, pp. 1–6, Jan, 2013.

[30] Wang, K., Liang, M., Wang, L., Tian, L., Zhang, X., Li, K., Jiang, T., "Altered functional connectivity in early Alzheimer's disease: a resting-state fMRI study," Hum. Brain Mapp, Vol. 28, No. 10, pp. 967–978, Oct, 2007.

[31] Supekar, K., Menon, V., Rubin, D., Musen, M., Greicius, M.D., "Network analysis of intrinsic functional brain connectivity in Alzheimer's disease," PLoS Comput. Biol., Vol. 4, No. 6, pp. e1000100, Jan, 2008.

[32] Yao, Z., Zhang, Y., Lin, L., Zhou, Y., Xu, C., Jiang, T., "Abnormal cortical networks in mild cognitive impairment and Alzheimer's disease," PLoS Comput. Biol., Vol. 6, No. 11, pp. e1001006, Nov, 2010.

[33] Kaufmann L., Ischebeck A., Weiss E., Koppelstaetter F., Siedentopf C., Vogel S. E., et al., "An fMRI study of the numerical Stroop task in individuals with and without minimal cognitive impairment," Cortex, Vol. 44, No. 9, pp. 1248–1255, Oct, 2008

[34] Teipel S. J., Meindl T., Grinberg L., Heinsen H., Hampel H., "Novel MRI techniques in the assessment of dementia," Eur. J. Nucl. Med. Mol. Imaging, Vol. 35, No. Suppl. 1, pp. S58–S69, Mar, 2008

[35] Thomann P. A., Schläfer C., Seidl U., Santos V. D., Essig M., Schröder J., "The cerebellum in mild cognitive impairment and Alzheimer's disease - a structural MRI study," J. Psychiatr. Res., Vol. 42, No. 14, pp. 1198–1202, Oct, 2008.

[36] Serrano-Pozo A., Frosch M. P., Masliah E., Hyman B. T. (2011). Neuropathological alterations in Alzheimer disease. Cold Spring Harb. Perspect. Med. 1:a006189

[37] Ni R., Gillberg P. G., Bergfors ., Marutle A., Nordberg A. (2013). Amyloid tracers detect multiple binding sites in Alzheimer's disease brain tissue. Brain 136, 2217–2227

[38] Birn, R.M., Diamond, J.B., Smith, M.A., Bandettini, P.A., "Separating respiratory variation-related fluctuations from neuronal-activity-related fluctuations in fMRI," NeuroImage Vol. 31, No. 4, pp. 1536–1548, Jul, 2006.

[39] Chang, C., Cunningham, J.P., Glover, G.H., "Influence of heart rate on the BOLD signal: the cardiac response function," NeuroImage, Vol. 44, No. 3, pp. 857–869, Feb, 2009.

[40] Shmueli, K., van Gelderen, P., de Zwart, J.A., Horovitz, S.G., Fukunaga, M., Jansma, J.M., Duyn, J.H., "Low-frequency fluctuations in the cardiac rate as a source of variance in the resting-state fMRI BOLD signal," NeuroImage, Vol. 38, No. 2, pp. 306–320, Nov, 2007.

[41] Wise, R.G., Ide, K., Poulin, M.J., Tracey, I., "Resting fluctuations in arterial carbon dioxide induce significant low frequency variations in BOLD signal," NeuroImage, Vol. 21, No. 4, pp. 1652–1664, Apr, 2004.

[42] Temujin Gautama, Danilo P Mandic, Marc M Van Hulle, "Signal nonlinearity in fMRI: a comparison between BOLD and MION," IEEE Transactions on Medical Imaging, vol. 22, no. 5, pp. 436–444, May. 2003.

[43] Danilo P. Mandic, Naveed ur Rehman, Zhaohua Wu, Norden E. Huang, "Empirical mode decomposition based time-frequency analysis of multivariate signals", IEEE Signal Processing Magazine, Vol 30, No 6, pp. 74-86, Nov. 2013.

[44] David Looney, Apit Hemakom and Danilo P. Mandic, "Intrinsic multiscale analysis: A multivariate empirical mode decomposition framework", Proceedings of the Royal Society A, Vol 471, No 2173, pp. 20140709, Jan. 2015.

[45] Ronghui Ju, Pan Zhou, Shiping Wen, Wei Wei, Yuan Xue, Xiaolei Huang, Xin Yang, "3D-CNN-SPP: A Patient Risk Prediction System From Electronic Health Records via 3D CNN and Spatial Pyramid Pooling,"

IEEE Transactions on Emerging Topics in Computational Intelligence, early access, pp. 1-15, Jan, 2020.

[46] Zhuoling Li., Minghui Dong, Shiping Wen, Xiang Hu, Pan Zhou, Zhigang Zeng, "CLU-CNNs: Object Detection for Medical Images," Neurocomputing, vol. 350, pp. 53-59, April, 2019.

[47] Rehman, N.U., Park, C., Huang N.E., et al., "Emd via memd: multivariate noise-aided computation of standard emd," Advances in Adaptive Data Analysis, vol. 5, no. 2, pp: 1350007, 2013,

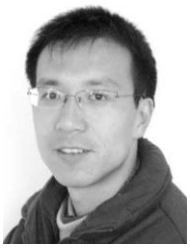

Haifeng Wu received the M.S. degree in electrical engineering from Yunnan University, Kunming, China, in 2004, and the Ph.D. degree in electrical engineering from Sun Yat-Sen University, Guangzhou, China, in 2007. He is currently a professor at the Department of Information Engineering in the Yunnan Minzu University. His research interests include neural signal processing, machine learning and mobile communications.

Lingxu Kong received the B.E. degree in electrical engineering from Yunnan Minzu University, Kunming, China, in 2018. She is currently pursuing his M. S. degree at the Department of Information Engineering at the Yunnan Minzu University. Her research interests include biomedical signal processing, machine learning.

Yu Zeng received the M.S. degree in electrical engineering from Yunnan University, Kunming, China, in 2006. She is currently an assistant professor at the Department of Information Engineering at the Yunnan Minzu University. Her research interests include wireless network, mobile communications.

Han Bao received the B.E. degree in electrical engineering from Yunnan Minzu University, Kunming, China, in 2018. She is currently pursuing his M.S. at the Department of Information Engineering at the Yunnan Minzu University. Her research interests include biomedical signal processing, machine learning